Neuro-Fuzzy Systems for Computer-Aided Myocardial Viability Assessment

F. Behloul, B. P. F. Lelieveldt, A. Boudraa, M. F. Janier, D. Revel, and J. H. C. Reiber*

***Abstract*—This paper describes a multimodality framework for computer-aided myocardial viability assessment based on neuro-fuzzy techniques. The proposed approach distinguishes two main levels: the modality-independent inference level and the modality-dependent application level. This two-level distinction releases the hard constraint of multimodality image registration. An abstract description template is used to describe the different myocardial functions (contractile function, perfusion, metabolism). Parameters extracted from different image modalities are combined to derive a diagnostic image. The neuro-fuzzy techniques make our system transparent, adaptive and easily extendable. Its effectiveness and robustness are demonstrated in a positronn emission tomography/magnetic resonance imaging data fusion application.**

***Index Terms*—Computer-aided diagnosis, data fusion, myocardial viability, neuro-fuzzy systems.**

I. Introduction

CORONARY artery disease is the most common cause of heart failure. It is recognized that heart failure and poor left ventricular (LV) function may improve after revascularization procedures, such as coronary artery bypass surgery or percutaneous transluminal coronary intervention. Several studies have demonstrated that a revascularization procedure is beneficial in patients with severe LV dysfunction in promoting their survival and improving their functional status. The success rate of such procedures however, relies on an accurate assessment of myocardial viability i.e., the capacity of the myocardium to recover from ischemic damage [1].

The decision as to which patient with coronary artery disease might benefit from revascularization procedures is difficult. Conventional imaging techniques in the preoperative examination of these patients [X-ray, computed tomography, Echo, magnetic resonance imaging (MRI)] allow the assessment of coronary artery anatomy as well as wall motion and ejection fraction. However, they fall short in giving useful information on the reversibility of dysfunctional myocardial segments. On the other hand, nuclear cardiology techniques (various T1-201 imaging protocols, PET assessment of myocardial metabolism, and more recently Tc-99m sestamibi and tetrofosmin imaging) have been evaluated extensively for their ability to predict reversibility of dysfunctional LV myocardium [2], [3]. By detecting the presence of a sufficient amount of viable myocardium, the potential candidate for revascularization may be identified.

Conventionally, the diagnostic approach on viability was binary: viable versus nonviable. More recent experimental studies have reported that myocardial dysfunction results from several ischemic processes (hibernation, acute stunning, chronic stunning, maimed myocardium, and necrosis) [1]–[4]. The concept of myocardial viability is not binary any more, although it is still vague and the different ischemic states are still difficult to identify in practice. In clinical routine, the question of viability faces many underlying questions: how viable is the myocardium? Is it expected to recover its contractile function? If yes, what is the average delay the recovery process should take? Are there different stages of recovery? These questions are not yet answered satisfactorily and are still subject to polemic discussions. To answer these questions, an accurate and detailed viability assessment is required.

The discrimination between the different ischemic processes requires information about myocardial perfusion, glucose metabolism, and inotropic reserve (IR) (i.e., contractile function improvement from rest to stress conditions). An accurate quantification (or assessment) of each function, currently, can only be obtained from multiple modalities. It is, thus, of major importance to combine the contractile function, the perfusion, and metabolism in a multimodality framework in order to characterize and understand the different ischemic processes. However, this results in a huge amount of data and images to analyze. For a physician, it is a significant problem to combine data provided by different modalities or even the same modality at different examinations. Because of the excessive quantity of data and ill-digested information, wrong (or nonreproducible) interpretations might result. There is obviously a need for automatic tools as an aid to process the data. Therefore, advanced information processing methods such as multiple source data fusion techniques [8] for computer aided diagnosis (CAD) are required.

Many applications of multimodality image fusion have been limited to the pixel or feature level [5]–[7]. The aim of such applications was mainly to superimpose images from different modalities in order to display inherent information in a single image. These applications require accurate image registration. The originality of this work lies in the fact that image fusion takes place at an abstract level (also called symbolic level). A decision process combines different parameters extracted from

Manuscript received June 1, 2001; revised November 1, 2001. *Asterisk indicates corresponding author.*

F. Behloul and B. P. F. Lelieveldt are with the Division of Image Processing (LKEB), C2S, Department of Radiology, Leiden University Medical Center, 2300 RC Leiden, The Netherlands.

A. Boudraa is with the Research Institute of the French Naval Academy LANVEOC POULMIC BP 600 F 29240 Brest-Naval, France.

M. F. Janier is with CERMEP, Centre d'Exploration et de Recherche Médicale par Emission de Positons, 59 boulevard Pinel, 69003, Lyon, France.

D. Revel is with the Research and Applications Center for Image and Signal Processing (CREATIS), 69003 Lyon, France.

*J. H. C. Reiber is with the Division of Image Processing (LKEB), C2S, Department of Radiology, Leiden University Medical Center, P.O. Box 9600, 2300 RC Leiden, The Netherlands (e-mail: J.H.C.Reiber@lumc.nl).

Publisher Item Identifier S 0278-0062(01)11216-4.

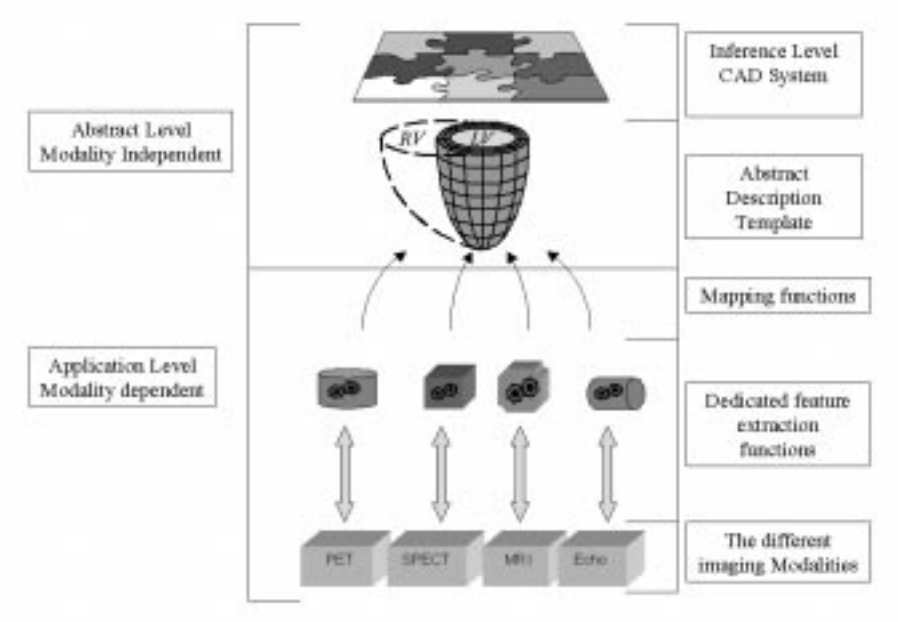

Fig. 1. Computer-aided viability assessment system structure. The proposed architecture has two main parts: the abstract level, which is modality independent and the application level which is modality dependent. Mapping functions are required to interface between the two parts.

different images (different studies or modalities) to derive a diagnostic image. This constitutes the main novelty of our work.

The structure of our CAD system is described in Fig. 1. The effectiveness of our solution lies in the fact that we distinguish two main levels: the abstract level and the application level. The abstract level captures the decision making process of a clinician. Based on the state-of-the-art in myocardial viability research, we defined an abstract description template (ADT) of myocardial functions (perfusion, metabolism and contraction) and viability. The ADT is modality independent; it is used as an interface between the inference level of the CAD system (where all the parameters are effectively combined) and any feature extraction software. At the application level, any imaging modality and/or protocol can be used. Dedicated software tools are used for the extraction of relevant parameters/features. In order to bring the extracted features to a higher level of inference, they are presented in the ADT format using mapping functions. The inference level of the CAD integrates the parameters and combines them with those derived from different modalities, studies or protocols, for an accurate viability assessment.

CAD systems are often required to process human-like expertise, to learn from examples to improve their performance, and/or extract new rules from data. Moreover, the user should always be able to verify the diagnostic conclusions, therefore, they should be transparent in the sense that they are able to explain how the diagnosis has been made. The quintessence of designing such intelligent systems lies in neuro-fuzzy computing. Neural networks (NNs) have the ability to learn and adapt themselves, while fuzzy set theory enables a transparent knowledge representation via fuzzy if–then rules. Moreover, fuzzy set theory provides a systematic calculus to deal with imprecise and incomplete information. The combined adaptivity and transparency of neuro-fuzzy networks motivated their use in this work for the design of the inference level of our CAD system.

In Section II, a detailed description of the abstract level of our CAD system is presented. Section III is dedicated to the application level. A PET–MRI data fusion is presented as an example. All the components of the application level corresponding to this example are presented, and discussed. General concluding remarks are discussed in Section IV.

II. CAD Abstract Level

The CAD abstract level captures the human expertise in myocardial viability assessment. It consists of a high-level reasoning system (the inference level), and a template of abstract description (ADT). The inference system has been designed based on a careful application of the neuro-fuzzy system. The reader may refer to [11] for a detailed presentation on the optimal design of such a fuzzy NNs. This section briefly introduces the neuro-fuzzy systems selected for our high-level reasoning system, and subsequently the ADT and the inference level are described in detail.

A. Neuro-Fuzzy Systems for CAD

Rule learning is an increasingly important topic in CAD and machine learning research. Machine learning concerns the development of algorithms or programs, which learn knowledge or skills. Given a set of corresponding input–output values of a system, the challenge consists of identifying and formulating the relations between the parameters and the diagnostic (input–output values) in order to automate the inference. When dealing with complex processes, it is generally not feasible to derive a functional input–output description. One needs to look for alternative methods. Fuzzy models described through fuzzy rules have proven to be a successful alternative. Indeed, general knowledge about actions or conclusions can be expressed by a set of fuzzy If–Then rules of a fuzzy inference system (FIS).

The basic structure of a FIS consists of three conceptual parts: a selection of fuzzy rules (rule base), definitions of the membership functions used in the fuzzy rules (dictionary), and a reasoning mechanism, which performs the inference based on given facts to derive a conclusion (a fuzzy reasoning). In general, one designs a FIS based on the past known behavior of the target system.

FISs have a well-structured knowledge representation. However, they are static models in the sense that they lack the adaptivity to deal with changing environments. NNs received the attention of the researchers because of their adaptivity and ability to learn. However, the semantic of a NN in terms of the problem to be solved is not explicit; the information is captured by a set of numerical values (connections weights) and NNs are, thus, considered as black box systems. It is clear that both models complement each other, making their combination an ideal solution.

Jang proposed a class of adaptive networks that is functionally equivalent to FISs [16]. Jang *et al.* [17] have shown that under simple conditions, a radial basis function NN (RBFN) is functionally equivalent to a FIS: while a FIS comprises a certain number of membership functions, a RBFN consists of RBFs. Both models produce a center-weighted response to small receptive fields, localizing the primary input excitation. The architectures proposed by Jang are referred to as the adaptive network-based FISs (ANFIS) or adaptive neuro-fuzzy systems.

The functional equivalence between RBFNs and FISs provides a shortcut for better design of both architectures [9]–[11]. In previous work, we have shown that the analysis and learning algorithms for RBFNs are applicable to FIS and that the fuzzy modeling procedure is a good way of initializing a RBFN before training [11], [15].

B. ADT

If one can standardize (at least within one institution) the way the different myocardial functions (contractile, perfusion and metabolism) are described and the number of myocardial segments to explore, multimodality data fusion for CAD can take place at an abstract level. The ADT has been designed for this purpose. It serves as an interface between the feature extraction procedures and the inference system, making the CAD inference level modality independent.

The ADT has two components: the spatial component and the semantic component. The spatial component concerns the description of the positions of the different myocardial segments under consideration, while the semantic component concerns the description of the myocardial functions and viability. The ADT has been defined with the help of two cardiologists, who were specialized in myocardial viability issues.

1) Spatial ADT: The spatial ADT is based on the concept of polar maps (or Bulls eye), which is widely used in nuclear image analysis [PET or single photon emission computed tomography (SPECT)]. Polar maps are a standard way of displaying myocardial functions and are well established in clinical settings. They are constructed by combining images from multiple planes [see Fig. 2(a)] so that information about the entire myocardium can be displayed in a single image. Polar maps can be compared to a three-dimensional cone-shaped heart activity image projected onto a single plane. Each image plane forms a ring in the polar map. The outer rings of the polar map correspond to the basal regions of the myocardium, whereas the inner rings correspond to the apical regions. In practice, the rings are divided into an arbitrary number of sectors (usually 60 in PET or SPECT). However, a clinician focuses on four (anterior, lateral, inferior, and septal) or six (anterior, anterior–lateral, inferior–lateral, inferior, inferior–septal, and anterior–septal) sectors for his visual interpretation of the image [see, Fig. 2(a) and (b)]. In our application, the number of sectors has been fixed by consensus. The rings are structured into 12 sectors [see Fig. 2(b)]. It makes the automatic diagnostic finer than the human one but still not too fine so that it allows the clinician to review the inference output step by step if required. Furthermore, a 12-sector partitioning allows the integration of other function quantification of lower resolution (e.g., segmental contractile function).

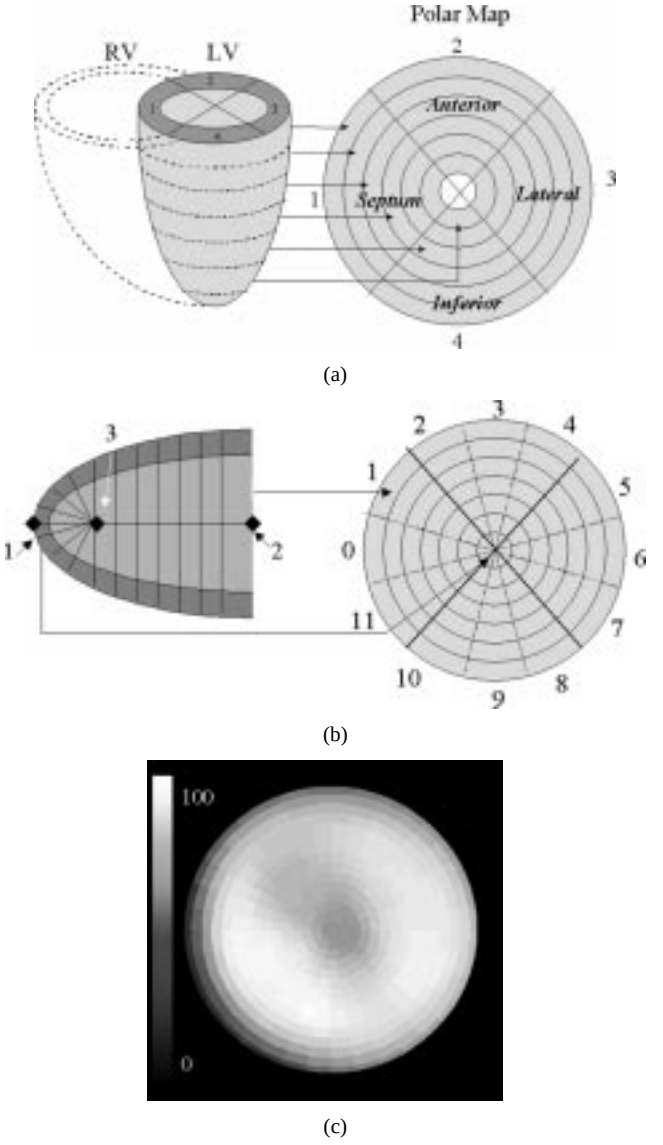

Fig. 2. The polar map representation. (a) The inner ring corresponds to the apex and the outer ring to the base. (b) Three points must be defined on the LV axis: the apex 1), the base 2) and a switch point 3). (c) Polar map with 36 sectors/ring. A color map is used to map the values of each sector.

Fig. 2(b) shows the way a polar map is constructed. Three points must be defined: the basal point, the apex and a switch

TABLE I
ADT VARIABLES AND THE CORRESPONDING LINGUISTIC VALUES

Variable	Linguistic values
Contractile Function at rest (CFr)	Akinetic/Dis-Kinetic (ADK), HypoKinetic (HK), and NormaL (NL)
Contractile Function under stress (CFs)	Higher (H), Equal (E) and Lower (L)
Inotropic Reserve (IR)	Ischemic (I), Function Improvement (FI), Hypo-kinetic with No Improvement under stress (HNI), A/Dis-kinetic and No Improvement under stress (ANI)
metabolism (FDG)	High (H), Medium (M) and Low (L)
Perfusion at rest (Pr)	High (H) and Low (L)
Perfusion under stress (Ps)	Higher (H), Equal (E) and Low(L)
Perfusion Reserve (PR)	Normal (NL), Ischemic (I) and Low (L)
Viability (Viab)	Necrosis (NE), Maimed (M), Metabolic Viable (MV), Viable (V), ISchemic (IS) and REmote (RE).

point where the sampling switches from linear to radial for the apical region. The myocardium contours are also required to limit the quantification or assessment of any function to the myocardial wall.

In order to integrate any function quantification (provided by the processing of any imaging modality) into the inference engine of our CAD system, one has to map the imaged area of the heart on the spatial template and provide for each sector of the mapped area a description of the function using the standard semantic template.

2) Semantic ADT: The semantic ADT consists of a list of linguistic variables, describing the different myocardial functions, and their corresponding linguistic values. The two cardiologists have been asked to list the different parameters that they consider while assessing myocardial viability. Seven variables were considered: the contractile function at rest (CFr); the contractile function at stress (CFs); the IR, derived from CFr and CFs; the perfusion at rest (Pr); the perfusion under stress (Ps); the perfusion reserve (PR), derived from Pr and Ps; the metabolism [the 18-fluorodeoxyglucose (FDG) uptake]. Table I summarizes the different variables and their corresponding abstract description (linguistic values).

The contractile functions at rest and under stress, the perfusion at rest and under stress and the FDG uptake, at this level of abstraction, are considered as input variables. The IR, the PR and the myocardial viability are inferred variables i.e., their values are defined using a reasoning mechanism and, thus, are considered as output variables. The FDG variable is the only quantitative one. For each segment the mean accumulation (or uptake) is calculated in percent (range: 0%–100%) of the segment with the maximal F-18 FDG accumulation. This segment is required to be perfused by a coronary artery with maximal 50% diameter stenosis, and/or to have normal wall motion. In clinical settings, FDG segments are predicted to be viable if the mean segmental F-18 FDG accumulation is at least 50% of the maximal accumulation. The segments are considered to be remote if the accumulation is at least 70% of the maximal accumulation.

All the other variables (CRr, CFs, IR, Pr, Ps, PR) take pure qualitative (linguistic) values. For computational and representational conveniences these variables are graded using fuzzy sets on a 100-point ordinal scale. All the fuzzy sets stipulating the linguistic variables have been defined and further tuned based on expert knowledge. Fig. 3 shows the membership

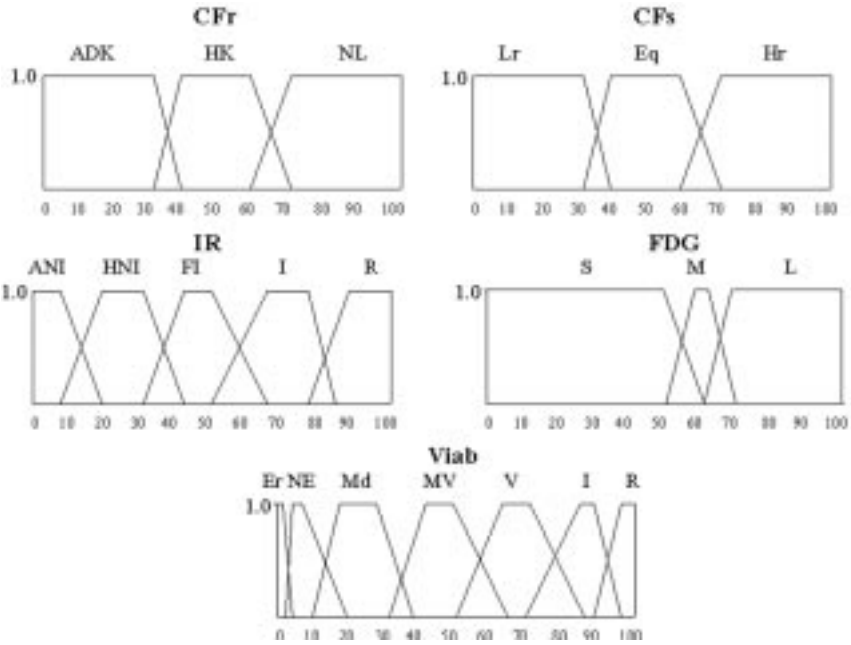

Fig. 3. Membership Functions stipulating the linguistic values of the variables CFr, CFs, IR, FDG, and $Viab$. These trapezoidal MFs have been defined and further tuned manually with the help of cardiologists.

functions corresponding to the variables considered in the application part of this paper (Section III).

In this paper, six levels of myocardial viability are distinguished: necrosis (not viable), maimed (probably not viable), metabolic viable (can show better FDG uptake after revascularization, but probably no contractile function improvement six months after revascularization), viable (shows contractile function improvement six months after revascularization), ischemic, and, finally, remote (for healthy myocardium).

C. The Inference Model

Once the variables of the system have been identified and their corresponding linguistic values and membership function have been defined, we had to find a way to combine these variables in order to derive a diagnostic on myocardial viability. In order to model expert knowledge, exploit redundancy and complementarity, deal with imprecise information, and ensure adaptability, ANFISs were selected to infer myocardial viability state from the different input variables.

The most straightforward way to use a ANFIS architecture in this context would be to design and train a five-input/one-output fuzzy NN. However, it is well known that the ANFIS model suffers from the curse of dimensionality [16], [17]. Furthermore, a large number of input variables decreases the interpretability of the ANFIS. Therefore, our system is a modular network of four cascaded ANFIS organized in a hierarchical way as shown in Fig. 4. This architecture mimics the way clinicians combine the variables to make a diagnostic on viability. Indeed, in order to investigate the contractile function, clinicians image the heart under normal condition (at rest with no effort) and then under stress (exercise stress or by injecting a pharmacological substance to stimulate the heart). The contractile functions (at rest and under stress) are then compared to evaluate the contractile reserve (IR). For example, in a normo-contractile myocardium, the heart is expected to have a higher contraction than under normal condition. Just like the clinicians, the CAD system combines contractile function at rest (Cr) and the contractile function under stress (Cs) in order to derive the IR using ANFIS1.

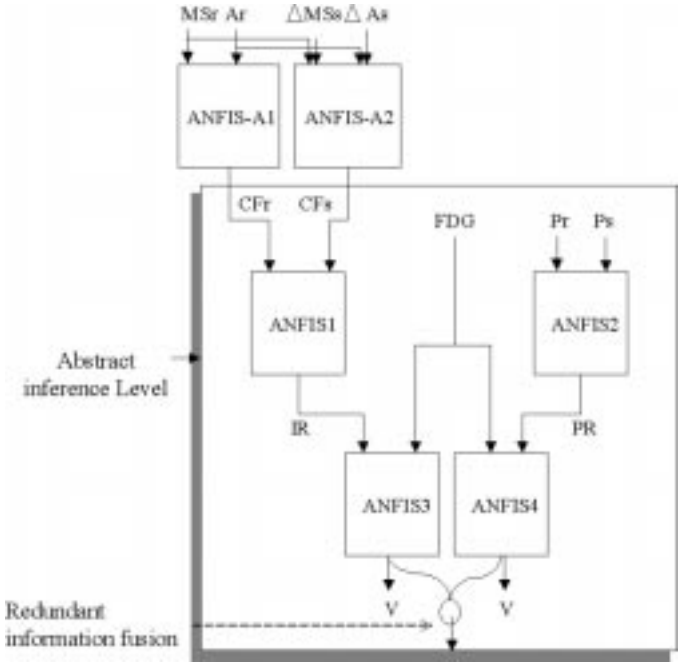

Fig. 4. Inference level of the CAD system. It consists of four modality-independent modules: ANFIS1 derives the IR by comparing the contractile functions at rest and under stress conditions. ANFIS2 assesses the PR by comparing the perfusion at rest and under stress conditions. The viability is assessed by combing the IR and the metabolism (ANFIS3) or by combining the PR and the metabolism (ANFIS4). Two extra modality-dependent modules are added for a PET–MRI data fusion application: ANFIS A1, for the assessment of the contractile function at rest from parameters describing the circumferential movement of the heart at rest, and ANFIS A2 for the assessment of the contractile function at stress circumferential movement parameters under stress.

The same applies to the PR: clinicians look at the myocardial perfusion at rest and then compare it with the perfusion under stress. A higher perfusion is generally expected for normo-perfused myocardium. A lower perfusion under stress is sign of ischemia. In our system, the PR is derived using ANFIS2 by combining the perfusion at rest (Pr) and the Perfusion under stress (Ps). Contractile function and perfusion examinations are carried out separately in practice. The corresponding measurements (or assessments) are independent; two different clinicians can investigate independently the two functions and then report to each other the outcome of their examination for a more complete diagnosis. Therefore, IR and PR are processed by separate modules in the CAD system.

For myocardial viability assessment a myocardial metabolism examination is often required. For an accurate diagnostic, it is routinely combined with a perfusion examination, and/or contractile function examination. The metabolism examination is often carried out by a nuclear physician on request of a cardiologist (or a cardio-radiologist). The outcome of the examination is later combined with that of the IR or PR. The combination of the three functions is ideal for an accurate diagnosis. Since the development of new metabolism imaging protocols that reflect also the perfusion (euglycemic hyperinsulinemic clamp infusion), a separate perfusion examination is not required in clinical settings, when FDG metabolism is imaged. However, for research settings, FDG examination is used as a gold standard for the evaluation of new perfusion imaging protocols (new MR sequences, new contrast agent). Thus, in our system, two separate modules for final accurate diagnosis are used. The myocardial viability is derived by combining IR and the FDG uptake (ANFIS3) or by combining the PR and the FDG uptake (ANFIS4). Depending on the available input variables, the system will use the corresponding ANFIS to derive a diagnosis on myocardial viability. For example: if the system has as input only perfusion and FDG uptake, then it will derive the viability assessment using ANFIS4. If only contractile function parameters are presented, then IR is derived. The system is input driven. It will go as deep as possible in the inference network. the deeper, the closer to an accurate viability assessment.

The ANFIS model is a hybrid architecture that can be considered as a particular RBFN or as a FIS. Depending on the available training data and prior knowledge, one will design and train them as NNs or as FISs. If no prior knowledge and fuzzy rules are available, then the design will be more NN oriented i.e., training on a consistent data set; the purpose of their use would be to extract rules from examples. However, if some expert rules combining input variables are available then FIS design techniques will be used. In this case, training is applied for further tuning of the rules and the fuzzy sets of systems. In this work, the cardiologist could provide fuzzy If–Then rules combining the input variables two-by-two. Fig. 5 shows the expert rules corresponding to the different ANFISs. The fuzzy If–Then rules of each ANFIS are summarized in a separate table. Each cell of a table corresponds to a fuzzy rule. For example:

The table in Fig. 5(a) corresponds to ANFIS1. It combines CFr and CFs to derive IR. The horizontal index of the table corresponds to the linguistic values of CFr and the vertical one corresponds to the linguistic values of CFs. The cells values

CFs \ CFr	NL	HK	ADK
L	I	FI	FI
E	R	HNI	ANI
H	R	HNI	ANI

(a)

PS \ Pr	H	L
H	NL	I
L	NL	L

(b)

FDG \ IR	ANI	HNI	FI	I	R
L	NE	M	Er	Er	Er
M	NV	MV	V	IS	Er
H	MV	MV	V	IS	RE

(c)

FDG \ PR	NL	I	L
L	Er	Er	M
M	Er	MV	MV
H	R	V	V

(d)

Fig. 5. ANFIS rules used by the inference level. The rules of each ANFIS are presented in a separate table. Each ANFIS has two input and one output variables. The linguistic values of the input variables are used to index the tables. The value of each cell is a linguistic value of the output variable that corresponds to the rule combining the two corresponding input linguistic values (a) ANFIS1: IR inference. (b) ANFIS2: PR inference. (c) ANFIS3: myocardial viability inference based on IR and FDG uptake values. (d) ANFIS4: myocardial viability inference based on PR and FDG uptake values.

are linguistic values of the inferred variable, in this case IR. The cell [NL, H] = R means *If CFr is NL (normal) and CFs is H (High) then IR is R (Remote)*.

An extra linguistic value, Er (Error), is used to express impossible combinations of input values [see Fig. 5(c) and (d)]. For example the combination:

If IR is R (Remote) and FDG is L (Low), then $Viab$ is Er (impossible). A normal myocardium is expected to have a high metabolic activity.

The inference system was tested by three different experts (two cardiologists and one biomedical researcher) in a simulation mode. In an online setting, experts were able to provide different values for the different parameters and check the output of the system. Identified cases of disagreement were used for a further manual tuning of the system (some fuzzy sets were narrowed and/or slightly shifted). The system was manually tuned until a 100% agreement score with the expert diagnosis was reached. This implies that the CAD system is able to mimic the

expert inference process. Therefore, no further training of the system was required. However, the system is designed so that it can potentially be retrained on new cases if required. The abstract level of inference is easily extendable. An extra module (ANFIS) combining IR and PR may be easily integrated.

The way CFr, CFs, Pr, and Ps are derived, is application dependent. Indeed, different modalities can be used to assess the contractile function. Depending on the spatial and temporal resolutions, different parameters can be considered. In Section III, we present an example of multimodality viability assessment where tagging MRI has been used to derive the contractile function parameters and PET for FDG uptake quantification. Two new ANFIS modules have been added to the CAD. These new modules required automatic training to extract rules and tune the corresponding fuzzy sets.

III. Application Level: PET–MRI Data Fusion

To demonstrate the benefit of our approach, we applied our CAD framework to a challenging PET–MRI data fusion problem. Tagging MRI and PET complement each other perfectly since the first allows an accurate contractile function analysis and quantification, while the second enables metabolism and perfusion quantification. In this paper, we will describe a contractile-function/metabolism fusion for the viability assessment.

A. PET and MRI Data Acquisition

PET images of FDG metabolism were acquired using a HR+ tomograph (Siemens Erlangen) scanner. The acquisitions were made during resting conditions and after euglycemic hyperinsulinemic clamp infusion. FDG (0.05 mci/kg) was injected as a slow bolus. A 3-D image (64 slices) taken 45 min after this infusion with 15 min acquisition time is considered. The spatial resolution of the 3-D image is: $x = 1.42$, $y = 1.42$, and $z = 2.4$ mm. Five patients with myocardial infarcts of different severity were considered in this application.

The contractile function is examined by tagging MRI using a single slice SPAMM sequence. The heart is imaged at rest and under pharmacological stress (10 μg·kg^{-1}·min^{-1} dobutamine infusion) through a maximum of seven short-axis images. The MR images were acquired using a Siemens vision 1.5-T scanner with the following protocol: 35-ms temporal resolution; 8-mm slice thickness; 45° and 135° tag orientations; FOV: 280 mm; TR: 70 ms; TE: 4 ms.

Nine healthy volunteers and 11 patients with myocardial infarcts were included in this study. An average of seven short-axis tagging MR images per patient (or volunteer) was acquired. As PET imaging is a relatively invasive protocol (injection of radio-active tracer), the healthy volunteers could not be scanned for FDG uptake images. From the 11 patients, only five had an additional PET examination (FDG uptake images). The reason for this is that the duo PET–MRI scanning is performed for research purposes and is not established in a clinical setting. This makes it difficult to gather a large data set. Therefore, the data of the nine healthy volunteers and six of the patients (those who did not get a PET image) were used for the training. The remaining data set was used for testing and validation.

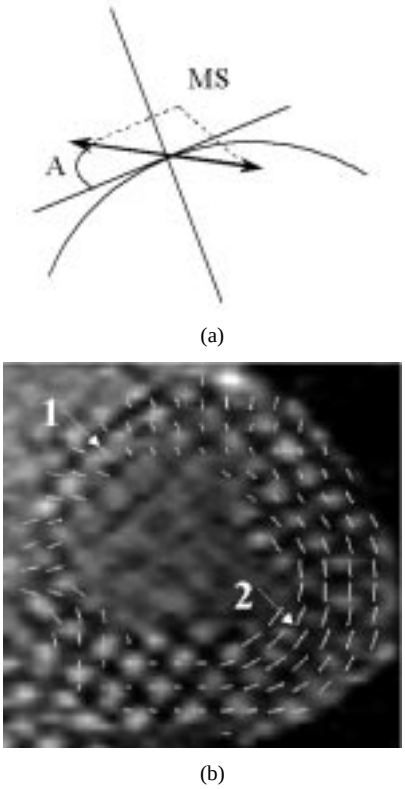

(a)

(b)

Fig. 6. Circumferential contraction assessment in tagging MRI (a): two parameters are considered: the Maximum Shortening (MS) of a myocardial element and the angle (A) of displacement. (b) Arrow 1 shows abnormal displacements: the region presents small values of shortening and a large angle. A normal myocardium is expected to have large shortening values in the circumferential direction (A should be small or nearly zero).

The two-dimensional contractile function parameters extraction was performed using an automatic contour and tag detection program, FINDTAGS [13]. This program allows the computation of strains at material points in the myocardium, based on the tag displacements over the heart cycle. A material point is defined as an infinitesimal volume of myocardial tissue. The mechanical state at a material point in the heart at any given imaging time is fully described by its deformation gradient tensor. The reader can refer to [14] for a complete description of the strain and deformation parameters computations.

In this study, we concentrated our analysis on the most important myocardial wall motion: the circumferential contraction. The maximum circumferential shortening (MS) of the deformation tensor and the angle (A) formed by the displacement vector versus the tangential direction are considered. MS is the largest eigenvalue of the deformation tensor, while A describes the orientation of the eigenvector corresponding to MS (see Fig. 6). A and MS are computed on rest images (Ar, MSr) and stress images (As, MSs) through several frames (an average of six time-slots for rest images, and four time-slots for stress images). The values corresponding to end-systole are considered.

B. PET–MRI Fusion System

The PET–MRI fusion system combines five input parameters (MSr, Ar, MSs, As, and FDG. In order to interact with the abstract inference level, CFr and CFs must be described in the ADT format. Therefore, two more ANFIS modules are

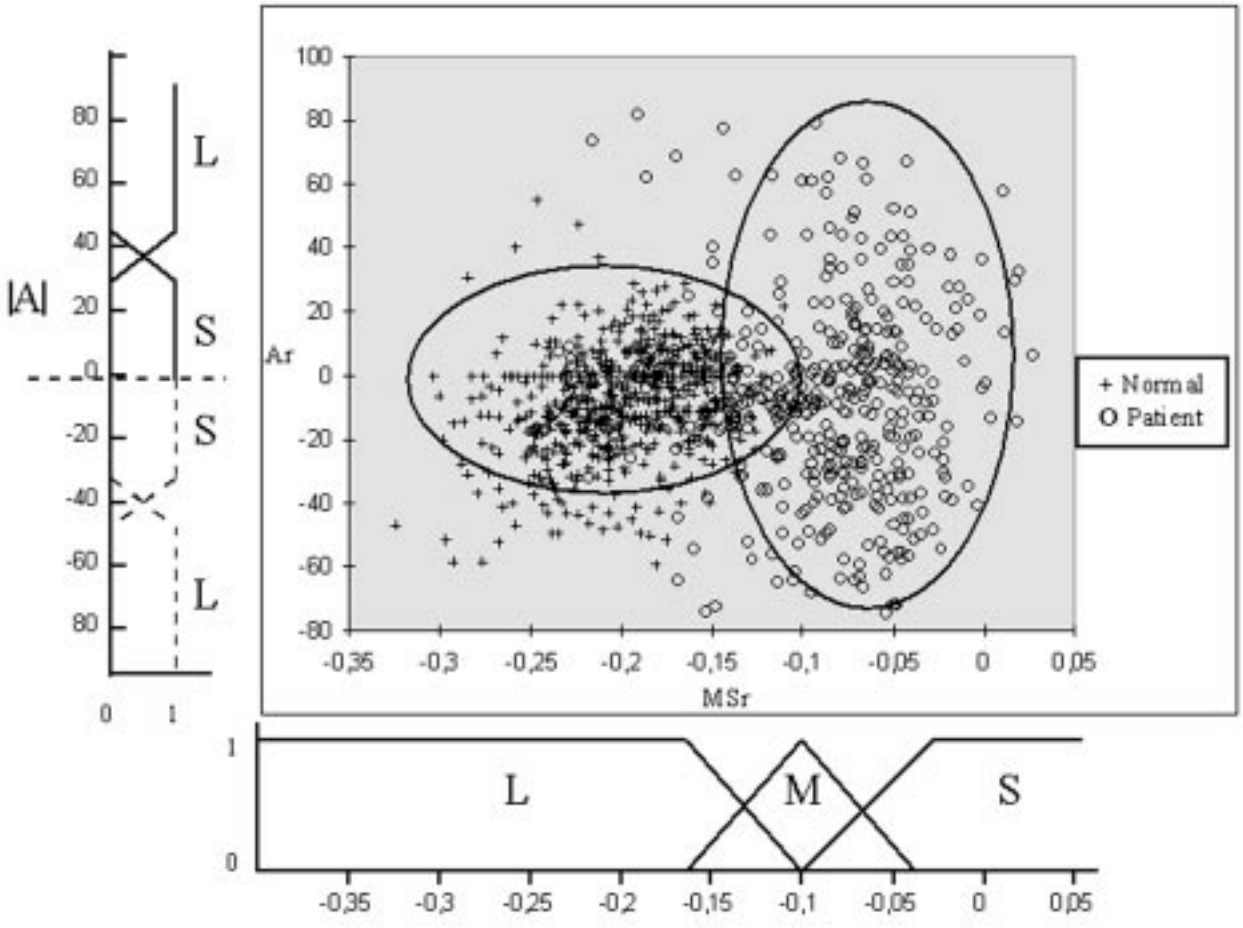

Fig. 7. The membership functions of MS and A at rest. The functions have been defined automatically using optimal fuzzy clustering. Only the absolute value of A (the amplitude) is considered. Healthy volunteers: MSr is generally over 0.15 in absolute value and Ar is within the interval $[-45°, +45°]$. For patients, MSr is generally smaller than 0.15 in absolute value and Ar can be outside $[-45°, +45°]$.

integrated in order to derive the two inferred variables CFr and CFs based on (MSr, /, Ar) and (MSs, As), respectively.

1) ANFIS-A1: MSr is described by three linguistic labels: small (S), medium (M), and large (L). Ar is described by two linguistic values: small (S) and large (L). The membership functions that stipulate the linguistic values of the input variables MSr and Ar have been defined automatically by training procedures based on optimal fuzzy clustering algorithms [11], [19]. Training was performed on the normal population ($9^* \sim 7^*12 = 708$ segments) to define the MFs corresponding to M and L for MSr and S for Ar. To derive the remaining MFs (S for MSr and L for Ar), the diseased population ($6^* \sim 7^*12 = 528$ segments) was added to the training data set. The MFs derived from the first training step (on normal population) were adjusted after training on the whole data set (patients + normal). The membership functions of MSr and Ar are shown in Fig. 7. The fuzzy If–Then rules of ANFIS-A1 are summarized in the table presented in Fig. 8(a). As training is not within the scope of this paper, we refer the reader to [11] for a detailed presentation of the training procedures used in this application.

2) ANFIS-A2: Assessment of CFs is expressed in comparison with CFr. A myocardium that does not increase its contractile function under stress is considered as pathological tissue. To assess CFs, ANFIS-A2 uses $\Delta MS = |MSs| - |MSr|$, $\Delta A = |As| - |Ar|$ as input values where $|x|$ is absolute value of x. ΔMS and ΔA are described using three linguistic values: negative (N); Zero (Z)

MSr \ Ar	S	L
S	ADK	ADK
M	HK	HK
L	NL	ADK

(a)

ΔMS \ ΔA	N	Z	P
N	H	L	L
Z	H	E	L
P	H	H	L

(b)

Fig. 8. Fuzzy rules corresponding to the modality-dependent (a) ANFIS-A1 and (b) ANFIS-A2.

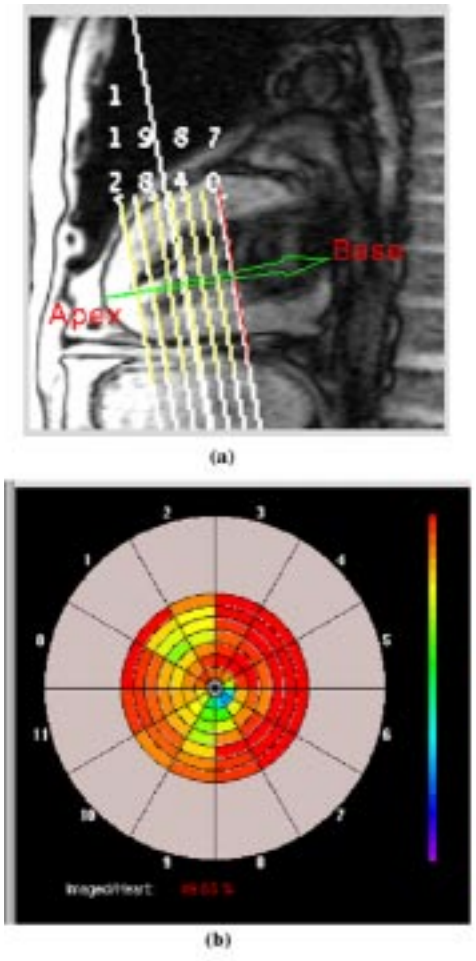

Fig. 9. Partial polar map. (a) An MRI scout view is used to point at the apex, the base, and first imaged plane. (b) The relative positions of the MRI plane on a partial polar map.

and positive (P). Fig. 8(b) shows the fuzzy If–Then rules of ANFIS-A2. The two ANFIS Module are pipelined with the abstract inference modules as shown in Fig. 4.

C. Mapping Functions to ADT

Before combining parameters extracted from different sources or modalities, one must make sure that the considered parameters refer to the same region (sectors in our case). In this approach, MRI parameters and FDG uptake parameters are mapped on the spatial ADT (a polar map). In MRI, the heart is generally covered through a set of slices. When short-axis tagging images are acquired, the most apical region is commonly not examined. In this case, only a partial polar map can be derived. In contrast to a polar-map, a partial polar map represents only a part of the ventricle. The mapping procedures must localize the imaged part and map it in a polar map where only the imaged segments are given a value. The nonimaged part is left blank [see Fig. 9(b)].

For this application, the mapping functions are integrated into a user-friendly interface where very few operator-interactions are required. In MR images, a long-axis scout view showing the position of the imaged slices is used [Fig. 9(a)]. The user has

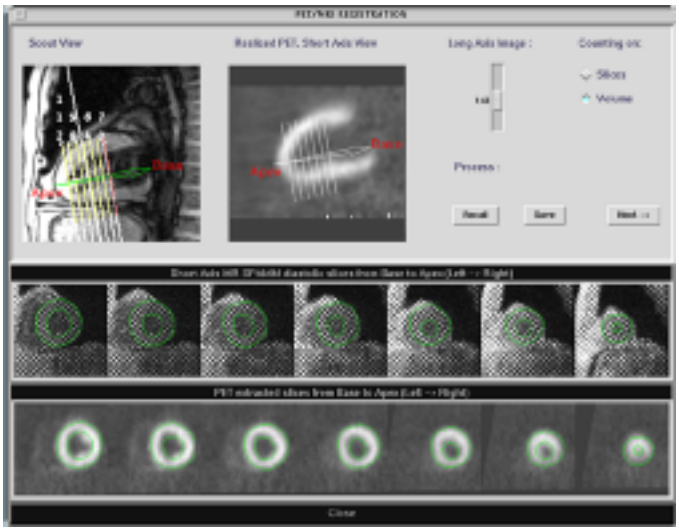

Fig. 10. User-friendly interface for partial polar map definition. The PET short-axis slices corresponding to the MRI slices are displayed. The automatically detected LV contours in MRI are mapped on the PET slices.

to define the apex, the base, and the position of the first plane (most basal). The position of the other planes is automatically defined using header information (slice thickness and interslice space). Knowing the relative positions of the planes on the LV axis, it is easy to map the corresponding rings on the partial polar map. The FDG uptake polar map can be calculated by the conventional methods. The intersecting parts with the MRI polar maps are considered for further automatic inference and diagnosis.

In this paper, only the part of myocardium imaged by MRI is considered. Thus, a partial FDG uptake polar map construction is sufficient. Furthermore, it is less computational demanding and requires less operator interactions. Therefore, the polar-construction process is customized in order to speed up the whole procedure.

The PET volume is automatically resliced (from transversal slices to short-axis slices) using the double oblique angles used in MRI (when available). Using pixel size information in PET and MRI, the images are normalized to the same pixel size. When the user has finished pointing at the apex, the base, and the first plan on the MRI scout view—an arrow (from apex to base) with the relative positions of the MR slices—appears on the scout view and on a long-axis PET view (from the resliced volume). By simple translation (click and drag), the user may position the arrow correctly on the PET image. The corresponding PET slices are than automatically extracted [see Fig. 10].

The conventional FDG uptake counting procedure uses image profiles (on ray scanning) to determine the position of the myocardium. In this paper, the automatically detected LV contours by FINDTAGS software, are used to delineate the myocardium in the PET images [see Fig. 10]. By click and drag, the user positions the LV contours on one slice (any one) and the rest of the contours corresponding to the rest of the slices are automatically positioned using the translation parameters derived from the manual positioning.

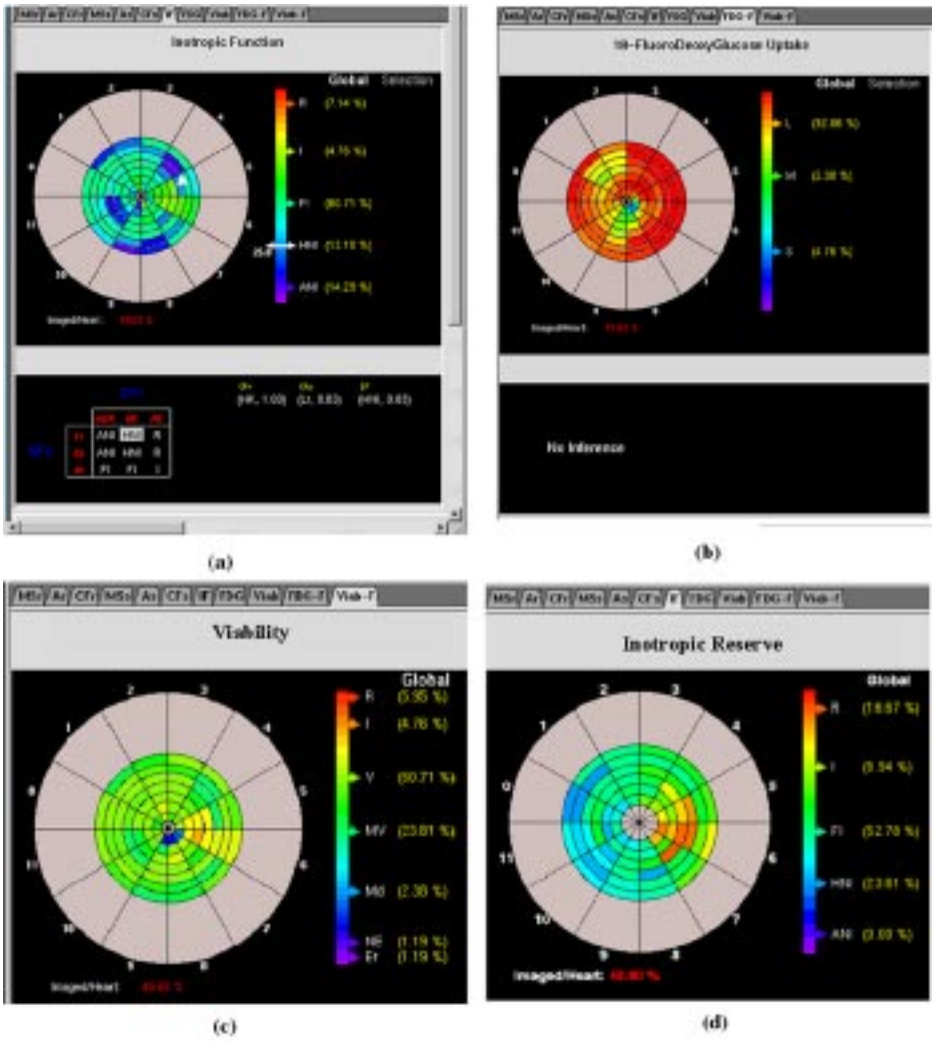

Fig. 11. CAD output for a patient with a small infarct in the apical region and a global contractile function defect. The polar maps of all the system parameters are presented in a notebook screen. Each page of the notebook shows the polar map and the corresponding inference rules (if any). By a simple click on a sector (see arrow) the exact value of the sector and the rule(s) used to infer it are displayed. (a) IR polar map. This patient presents a relatively good IR. (b) FDG-uptake polar map. Only a small defect is present at the apical region (4.76%). (c) Viability polar map. The CAD derived 61% of viable sectors and 24% of metabolic viable sectors. (d) IR after reperfusion. The heart shows a global IR improvement.

D. Results and Discussion

The system has been tested on 468 sectors from five patient data sets. The patients underwent extra examinations (angiography and/or SPECT perfusion examination), which were used by the experts for their diagnosis. An average of seven slices per patients was acquired. The polar maps presented approximately seven rings of 12 sector each. The inference level was applied to derive a viability diagnosis on a total of 468 sectors.

The Kappa statistic [20] was used to measure pair wise agreement between the CAD system and the cardiologists. The Kappa coefficient (K) is computed as follows:

$K = (P(A) - P(E))/(1 - P(E))$ where $P(A)$ is the portion of times the expert agreed with the CAD system and $P(E)$ is the number of times expected to agree by chance. For a complete instruction on how to compute K, see [20]. When there is no agreement other than that which would be expected by chance, K is zero. When there is total agreement K is one.

The obtained values in our case are: $P(A) = 91.67\%$, $P(E) = 35.42\%$, and $K = 0.8710$ which indicates a very good agreement. Two patient examples with infarction of different severity are presented in Figs. 11 and 12.

Fig. 11 shows the analysis of a patient presenting a small infarct in the apical region and relatively low IR in many myocardial sectors. The FDG polar map shows many sectors with high FDG uptake. The viability polar map shows enough viable myocardium especially around the infarcted region (blue sectors). Therefore, the patient underwent a revascularization procedure. An MRI examination has been carried out seven months after revascularization. Fig. 11(d) shows the polar map of the IR. Many sectors showed a better IR and the global contractile function of the heart was improved. On the right of each polar map, an exact quantification of the amount of the different myocardium-tissue classification is provided. The values represent a relative percentage to the imaged part of the heart. The size of the imaged part is given below the polar maps.

Fig. 12 shows the results obtained for a patient with a severe myocardial infarction. Very few viable myocardium is shown in the viability polar map [Fig. 12(c)]. Indeed, the IR polar map [Fig. 12(a)] showed little reserve in only few sectors and the

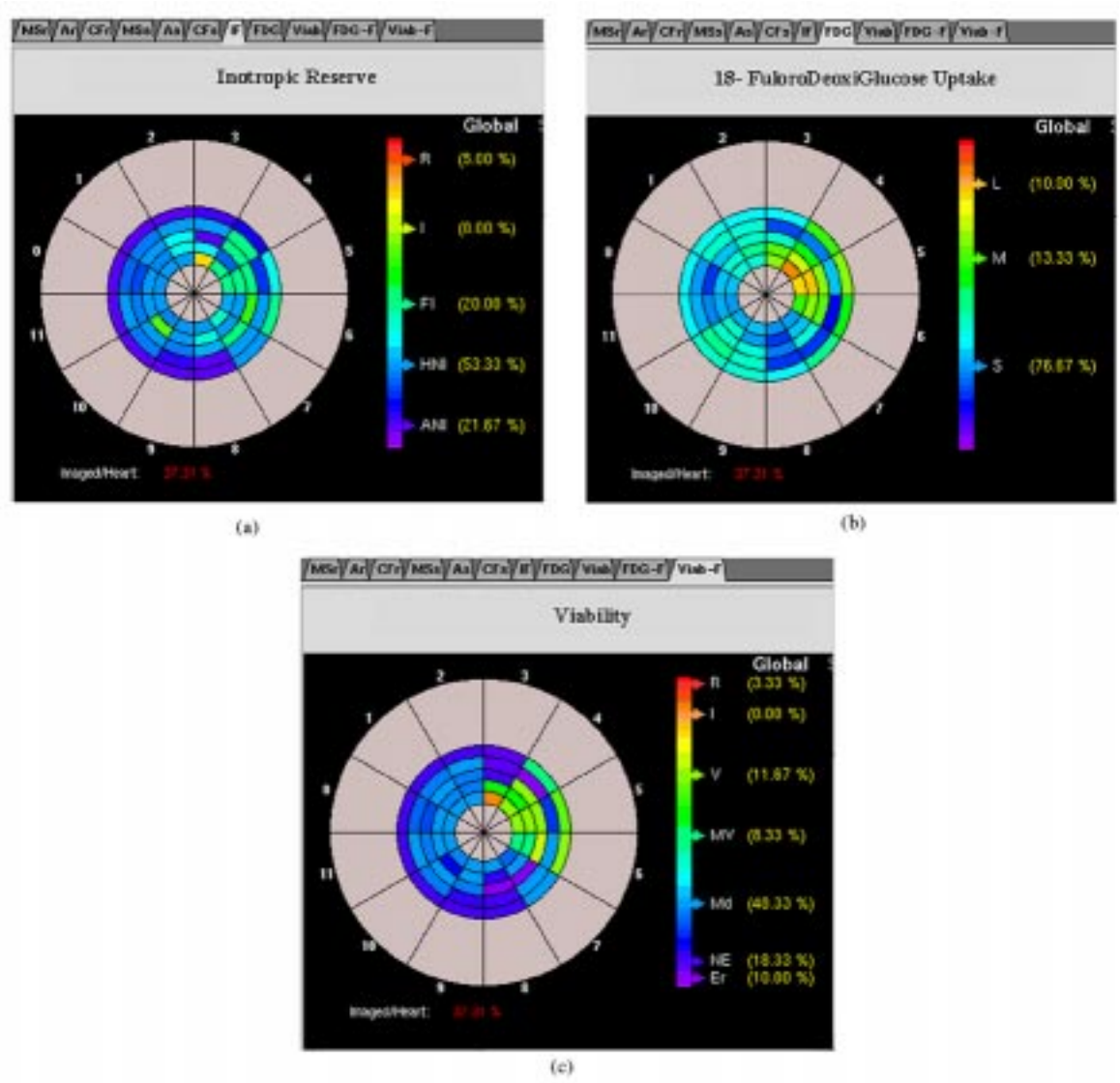

Fig. 12. CAD output for a patient with a severe myocardial infarction. The large majority of sectors showed a very poor (a) IR and (b) FDG-uptake polar map. Only the septal wall showed metabolic activity. (c) Viability polar map. The CAD system indicates only 12% of the imaged heart as viable and 8% as metabolic viable. Therefore, this patient was not considered a candidate for reperfusion but for cardiac transplant.

FDG uptake polar-map [Fig. 12(b)] showed very little uptake. (See the exact quantification on the right of the polar maps in the figures.) This patient was not considered to be a good candidate for revascularization due to the absence of viable myocardium.

The entire viability assessment, including the user interactions, does not exceed 2 min (on a Pentium II 450 Mhz). An accurate diagnosis is presented in a user-friendly interface. Polar maps of all the system variables are presented in a note-book window (see, Figs. 11 and 12). The physician can follow the fusion process step by step for a better understanding of the final result. By a simple click on a sector, the corresponding numerical value is displayed on color scale bar. If it concerns an inferred variable, the rules that have been used to derive the value are also displayed with the corresponding membership degrees [see Fig. 11(a)].

The main limitation of this application is that combined tagging MRI and PET examinations are not very common. Therefore, the number of data sets available for this study was relatively small, although continuously expanding. Currently, the particular application is used to demonstrate the potential of our CAD system, and it is mainly applied in clinical viability research. As yet, it is a valuable scout application for a better characterization of myocardial viability and a better understanding of the different ischemic processes. However, the fusion framework is also applicable to the widely applied combination of MRI and SPECT image data, which is a topic of ongoing research work.

IV. Conclusion

In this paper, a CAD system for myocardial viability assessment is presented. Neuro-fuzzy techniques have been used to develop a system that uniquely combines transparency with adaptivity. A general CAD framework based on multimodality data fusion has been proposed. The system is structured into two main parts: the modality-independent inference level, that captures the expertise in decision making on myocardial viability, and the modality-dependent application level that

encompasses segmentation/quantification procedures and mapping functions into the ADT. This two-level discrimination makes our CAD framework suitable to integrate any modality examination for myocardial viability studies.

The concept of an ADT proved to greatly simplify the multimodality and/or multistudy integration and fusion. The semantic ADT consists of a list of variables and the corresponding fuzzy linguistic values. It can be viewed as a nomenclature to use when describing the myocardial functions and viability. It is extendible and still open to modifications. The spatial ADT releases the hard constraint of image registration, which has been a real obstacle for multimodality image fusion and multimodality CAD in general. In this paper, we show that a pixel/voxel level registration is not mandatory. The idea of polar maps, widely used in nuclear imaging, demonstrated to be a very good frame for multimodality-based CAD. The pixel/voxel level image registration is replaced by image-to-ADT mapping functions. The spatial ADT resolution can be finer or coarser by increasing or decreasing the number of sectors (12 in this application), if finer or coarser mapping functions are available. This does not affect the inference level, as the inference is performed on a sector base.

The inference level remains unchanged for different applications. Being rule based, our CAD is easy to understand, as it can describe step by step the decision process. Since many variables (with different stages and combinations) are required for an accurate viability diagnosis, our CAD system has been made modular. A hierarchy of adaptive rule-based modules (ANFIS) is used. Each module can be further tuned or modified independently from the others, in the limit of the ADT (i.e., no new linguistic values are introduced). If new linguistic values are required, then modules using these values must be modified as well. The modular hierarchy is easily extendible (as shown in the presented application).

The effectiveness of our CAD system has been demonstrated through a particular application where PET and tagging MRI data fusion has been considered. The system performed very well and it is currently applied in several myocardial viability research studies. Further applications involving integration of MRI and SPECT are under development. Moreover, further development and updating of the semantic ADT is ongoing.

REFERENCES

[1] R. C. Marshall, J. H. Tilisch, M. E. Phelps, S. C. Huang, R. Carson, E. Henz, and H. R. Schelbert, "Identification and differentiation of resting myocardial ischemia and infarction in man with positron emission tomography, 18F-labeled fluorodeoxyglucose and N-13 ammonia," *Circulation*, vol. 67, pp. 766–778, 1983.

[2] H. R. Schelbert, "Metabolic imaging to assess myocardial viability," *J. Nucl. Med.*, vol. 35, pp. 8–14, 1994.

[3] S. H. Rahimtoola, "From coronary artery disease to heart failure: Role of the hibernating myocardium," *Amer. J. Cardiol.*, vol. 75, pp. 16–22, 1995.

[4] N. Hattori, S. Nekolla, K. Odaka, F. Bengel, and M. Schwaiger, "Utility of regionalEndocardial wall motion from gated FDG-PET to assess myocardial viability," *J. Nucl. Med.*, vol. 40, no. 5, Suppl.: 45P, 1999.

[5] S. Nekolla, U. Schricke, F. Roder, and M. Schwaifer, "Multitracer and multimodal coregistration and fusion in static and gated cardiac studies," *J. Nucl. Med.*, vol. 39, no. 5, 573, 145, 1998.

[6] S. Nekolla, S. Kneifel, J. Schneider-Eicke, J. Neverve, H. Daschner, G. Schröter, and M. Schwaiger, "Coregistration of gated MR and gated SPECT heart imaging: Functional overlay of morphology and perfusion," in *Proc. 3rd Meeting SMR, Nizza*, R. S. Balahan, Ed. Nizza, Aug. 19–25, 1995, vol. 725.

[7] A. Guimond, A. Roche, N. Ayache, and J. Meunier, "Three-dimensional multimodal brain warping using the demons algorithm and adaptive intensity corrections," *IEEE Trans. Med. Imag.*, vol. 20, pp. 50–69, 2001.

[8] M. A. Abidi and R. C. Gonzalez, *Data Fusion in Robotics and Machine Intelligence*. Boston, MA: Academic, 1992.

[9] K. M. Lee, D. H. Kwak, and H. Leekwang, "Tuning of fuzzy models by fuzzy neural networks," *Fuzzy Sets, Syst,*, vol. 76, no. 1, pp. 47–62, 1995.

[10] J. S. Jang, C. T. Sun, and E. Mizutani, *Neuro-Fuzzy and Soft Computing: A Computational Approach to Learning and Machine Intelligence*. Englewood Cliffs, NJ: Prentice-Hall, 1997.

[11] F. Behloul, B. P. F. Lelieveldt, A. Boudraa, and J. H. C. Reiber, "Optimal design of radial basis function neural networks for fuzzy-rule extraction in high dimensional data," *Pattern Recogn.*, vol. 35, no. 3, pp. 659–675, 2001.

[12] F. Behloul, A. Boudraa, B. P. F. Lelieveldt, M. Janier, and J. H. C. Reiber, "Myocardium extraction in positron emission tomography based on soft computing," *Comput. Med. Imag. Graph.*, vol. 25, pp. 277–286, 2001.

[13] M. A. Guttman, J. L. Prince, and E. R. McVeigh, "Tag and contour detection in tagged MR images of the left ventricle," *IEEE Trans. Med. Imag.*, vol. 13, pp. 74–88, Mar. 1994.

[14] W. G. O'Dell, C. C. Moore, W. C. Hunter, E. A. Zerhouni, and E. R. Macveight, "Three dimensional myocardial deformations: Calculation with displacement field fitting to tagged MR images," *Radiology*, vol. 190, pp. 829–895, 1995.

[15] F. Behloul, A. Boudraa, M. Janier, and R. Unterreiner, "Self-organized radial basis function network using fuzziness measures for object extraction in positron emission tomography images of the heart," presented at the Information Processing and Management of Uncertainty in Knowledge-Based Systems Conf., Paris, France, 1998.

[16] J. S. R. Jang, "ANFIS: Adaptive-network-based fuzzy inference systems," *IEEE Trans. Syst. Man, Cybern.*, vol. 33, pp. 665–685, May/June 1993.

[17] J. S. R. Jang and C. T. Sun, "Functional equivalence between radial basis function networks and fuzzy inference systems," *IEEE Trans. Neural Networks*, vol. 4, pp. 156–159, Jan. 1993.

[18] T. Takagi and M. Sugeno, "Fuzzy identification of systems and its application to meddling and control," *IEEE Trans. Syst., Man, Cybern.*, vol. SMC-15, pp. 116–132, 1985.

[19] I. Gath and A. B. Geva, "Unsupervised clustering algorithms," *IEEE Trans. Pattern Anal. Machine Intell.*, vol. PAMI-11, pp. 773–781, 1989.

[20] S. Siegel and N. J. Castellan, Jr., *Nonparametric Statistics for the Behavioral Science*, 2nd ed. New York: McGraw-Hill, 1988.